



Cite this: *RSC Adv.*, 2020, 10, 4404

Insight into the factors controlling the equilibrium of allylic azides†

Margarita M. Vallejos *^a and Guillermo R. Labadie ^{bc}

Several allylic azides with different double bond substitutions were studied to understand the factors, governing their equilibrium using density functional theory along with the quantum theory of atoms in molecules, non-covalent interactions and natural bond orbital approaches. The results showed that the hydroxyl group or heteroatoms in allylic azides interact with the molecule through an electrostatic weak interaction in each pair of regioisomers. The equilibrium shifts of substituted allylic azides, compared to non-substituted allylic azides, were not attributed to the presence of specific interactions, such as hydrogen bonds. The observed equilibrium shifts stemmed mainly from the strengthening and weakening of negative hyperconjugative interactions, which were affected by the weak interaction involving the proximal substituent in each regioisomer. A good linear correlation was obtained between the hyperconjugative energies of $\pi\text{C}=\text{C} \rightarrow \sigma^*\text{Z}_b$ interactions and the calculated percentages of the secondary azide and tertiary azide in the equilibrium mixture. Also, the effect of the aromatic ring substituent was analysed using such approaches. This study not only provides insights into the factors controlling the stabilities of the substituted allylic azides, but also settles the basis to predict the regioisomer predominance in the equilibrium mixture.

Received 2nd December 2019
Accepted 26th December 2019

DOI: 10.1039/c9ra10093h

rsc.li/rsc-advances

Introduction

Organic azides are versatile substrates for use in reactions such as the Staudinger reaction, Schmidt reaction and Curtius rearrangement.^{1–3} Also, since the introduction of copper(I) azide-alkyne cycloaddition, thousands of compounds have been prepared.^{4–6} Azide bioorthogonality has promoted this functional group's introduction on metabolites and proteins in many different studies.^{7–10}

Allylic azides are the building blocks for the synthesis of many natural products and nitrogen-containing heterocycles of pharmacological relevance.^{11–14} Despite the importance of these useful synthons, their applicability in synthetic schemes has been difficult due to their existence as regioisomeric mixtures that interconvert rapidly at room temperature, thus being, in general, inseparable (Fig. 1).^{15,16} The allylic azide rearrangement was first reported by Gagneux, Winstein and Young in 1960

(known as Winstein's rearrangement).¹⁵ Lately, Vanderwerf and Heasley¹⁷ found that tertiary and secondary allylic azides rearrange faster than the primary ones existing in the equilibrium mixture, leading to a predominant population of the latter.

Allylic azide rearrangements are controlled by thermodynamic stabilization of the more substituted $\text{C}=\text{C}$ double bond. Also, the distribution of the regioisomers is affected by the steric bulkiness and the conjugations of the double bonds. It has widely been assumed that the rearrangement of the allylic azides occurs through a concerted [3,3]-sigmatropic mechanism via a cyclic transition structure.^{18,19} However, an ionic mechanism was recently proposed for the rearrangement of allylic azides at high temperatures or under Lewis acidic conditions.²⁰

It is necessary to control the thermodynamic ratio of the regioisomeric azides, which generally depends on the substrate, in order to be synthetically useful.²¹ Different groups have studied the rearrangement of substituted allylic azides to

^aLaboratorio de Química Orgánica, IQUIBA-NEA, Universidad Nacional del Nordeste, CONICET, FACENA, Av. Libertad 5460, Corrientes 3400, Argentina. E-mail: vallejos.marga@gmail.com; m.vallejos@conicet.gov.ar; Tel: +54-379-4457996 ext. 104

^bInstituto de Química Rosario, UNR, CONICET, Suipacha 531, S2002LRK, Rosario, Argentina

^cDepartamento de Química Orgánica, Facultad de Ciencias Bioquímicas y Farmacéuticas, Universidad Nacional de Rosario, Suipacha 531, S2002LRK, Rosario, Argentina

† Electronic supplementary information (ESI) available: Relative Gibbs free energies for the regioisomers 1 and 2. Free energy profiles for the [3,3]-sigmatropic rearrangement, topological properties and Cartesian coordinates of azides under study. See DOI: 10.1039/c9ra10093h

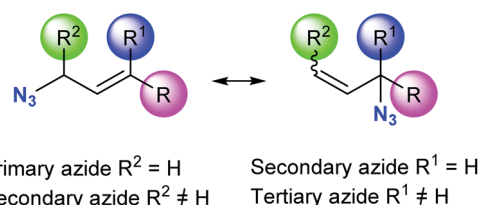


Fig. 1 [3,3]-Sigmatropic rearrangement of allyl azides.



understand the main factors governing the equilibrium. Sharpless and co-workers²² noted that the equilibrium of hydroxylated allyl azides was shifted towards secondary azides compared to the parent aliphatic azide (Scheme 1b). This shift was attributed to the formation of hydrogen bonds between the hydroxyl and azide groups.^{22–24} Recently, Topczewski and co-workers²⁵ observed that a silyl-protected analogue of hydroxyl-crotyl azide also showed a similar shift towards branched regioisomers with the OR group close to the azide group (Scheme 1c).

The allylic azide equilibrium ratio might be also significantly biased by an aromatic ring substituent. Overall, only conjugated regioisomers with the aromatic ring have been evidenced.^{26,27} We previously performed a theoretical study using density functional theory and the quantum theory of atoms in molecules (QTAIM) approach^{28,29} to rationalize the experimental results. Those results showed a high dependency of the double bond substitution on the prenylazides with different chain lengths of the prenylazide. Topological analysis of the electron-charge density revealed that the effect of the aromatic substituent was strictly electronic, with scarce or null contribution from the steric factor.³⁰

There are few computational studies on the allylic azide rearrangement and most of these have been based on the energetic and geometric parameters to analyse the effects that control the equilibrium.^{23,31} Herein, several representative allylic azides (alkyl, aryl and hydroxylated allylic azides) with different degrees of substitution on the double bond were chosen to study the effects of the substituent group on the stabilization of the regioisomers. Such effects were evaluated using the quantum topological methods by means of the QTAIM and non-covalent interactions (NCI) analyses and natural bond orbital (NBO) analysis.^{32,33} The obtained results provide a better understanding of the factors that govern the equilibrium, and might help predict the regioisomer composition of allylic azides in the equilibrium.

Methodology

All the geometries were optimized with the M06-2X³⁴ functional and the 6-31+G(d,p) basis set. Single-point energies were calculated with the larger 6-311++G(d,p) basis set and the implicit SMD³⁵ solvation model with chloroform as the solvent. This level of theory for the calculation was chosen after an initial study for azides **1** and **2** using different DFT functionals (M06-2X,³⁴

B3LYP^{36,37} and MPWB1K³⁸) in conjugation with the 6-31+G(d) and 6-311++G(d,p) basis sets in the gas phase for the optimization and frequency calculation and 6-311++G(d,p) for the single-point calculation in chloroform (see ESI†). The reported free energies were calculated at 298.15 °K and 1 atm in chloroform.

As was established, the Winstein rearrangement is thermodynamically controlled, so this study focused on the regioisomers; however, for each reaction, the transition structure was localized (see ESI†). The calculated free energy barriers for the rearrangements of the azides under study were relatively low (<30 kcal mol^{−1}), indicating that those could spontaneously occur at room temperature. Frequency calculations were computed to verify the nature of the stationary points as true minima or as first-order transition structures and to evaluate the thermal corrections. The intrinsic reaction coordinate (IRC) was further performed to check the energy profiles connecting each TS to the two associated minima.

Topological analyses were carried out with QTAIM²⁸ and non-covalent interactions (NCI), using the AIMALL³⁹ and NCIPLOT 3.0 (ref. 40) programs, respectively. Hyperconjugative interactions were evaluated using the Natural Bond Orbital program (NBO 3.1).⁴¹

Results and discussion

The present study report is divided into three sections according to the types of allylic azides: primary vs. secondary, primary vs. tertiary and secondary vs. secondary. The percentage of *cis* isomer in the equilibrium mixture was generally low (or negligible) and therefore it was not computed for practicality.

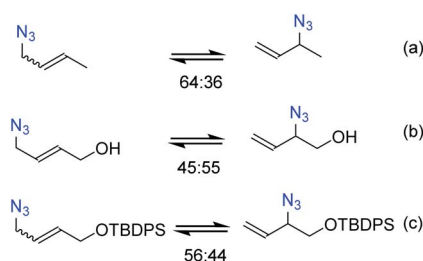
Primary vs. secondary azides

The relative Gibbs energies, and the experimental and calculated equilibrium ratio for the azides under study are summarized in Table 1.

Table 1 Relative free energies (ΔG , kcal mol^{−1}) and calculated and experimental equilibrium ratios for the azides under study^a

Azide (X)	R ₁	ΔG (X _b – X _a)	X _a : X _b ratio	
			Calcd ^a	Exp. ^{b,c}
1	Me	1.10	86 : 14	67 : 33 (ref. 22)
2	CH ₂ OH	−0.02	49 : 51	45 : 55 (ref. 22)
3	OTMS	0.67	75 : 25	56 : 44 (ref. 25)
4	Ph	3.72	100 : 0	100 : 0 (ref. 30)

^a Ratios were computed using Boltzmann factors based on ΔG . ^b **1a** (57% *E-trans*, 10% *Z-cis*). ^c The experimental data for azide **3** correspond to hydroxyl-crotyl azide derivative –OTBDPS, structurally similar to –OTMS, **3a** (52% *E-trans*, 4% *Z-cis*).



Scheme 1 Equilibrium distribution of (a) crotyl azide, (b) hydroxyl-crotyl azide and, (c) its silyl-protected analogue.



The primary azides **1a**, **3a** and **4a** were more stable by 1.10, 0.67 and 3.72 kcal mol^{−1} than the corresponding secondary ones, being the calculated ratio $X_a : X_b$ in agreement with the experimental results. Also, for azide **1**, it was in accordance with the previous calculation at other levels of theory.^{25,42} The energy difference between **2a** and **2b** was lower, providing a ratio that slightly favoured the second. In some cases, the energy difference between both regioisomers was smaller than 1 kcal mol; however, the calculated ratios indicated a shift towards the secondary azides for **2** and **3** compared to **1**, which correlated well with the observed equilibrium trend.

In azide **2b**, the OH group is directed towards N³ ($d_{H\cdots N} = 2.38$ Å; $\angle OH\cdots N^3 = 107^\circ$), which could be a hydrogen bond or a coulombic interaction as was previously proposed to explain the equilibrium shift. To obtain more information about this interaction, a topological analysis of the electron density based on the QTAIM was performed. This approach is one of the most popular for assessing whether a hydrogen bond is present. From this approach, the presence of a bond critical point, bcp (3,−1), between a hydrogen bond donor group and a hydrogen bond acceptor group along the bond path connecting two interacting atoms is considered to be a characteristic of hydrogen bonding.⁴³ The molecular graphs of the azides are depicted in Fig. 2 (the topological properties evaluated at the bcps are listed in Table S2, in the ESI†).

According to the QTAIM analysis (Fig. 2), no bcp was observed between the hydrogen of the OH group and the N³ atom in **2b**. On the basis of this theory, this may indicate that there was no hydrogen bond interaction in the **2b** regioisomer. However, there are some criticisms of the interpretation of

QTAIM theory, particularly for weak long-range bonds like hydrogen bonds.⁴⁴

The NCI index is based on the electron density and its derivatives and this approach allows the identification of non-covalent weak interactions in a molecular system, particularly those interactions that cannot be revealed from an analysis of the density values.⁴⁵ The NCI plot enables the visualization through the space of the gradient isosurfaces and provides qualitative information on the interacting molecular regions.

For azide **2b**, the NCI plot shows a green isosurface between the hydrogen of the OH group and N³, indicating the presence of a weak interaction. Within the NCI framework, the OH \cdots N interaction in 2-aminoethanol, with no bcp, was characterized as a weak hydrogen bond by the presence of a blue-green isosurface between the OH and NH₂ moieties, which is different from that observed for **2b**.^{46,47} Also, the NCI plot shows a similar green isosurface between the oxygen of the OH group and the hydrogen atom H² in the **2a** regioisomer ($d_{H\cdots O} = 2.37$ Å; $\angle C^2H^2\cdots O = 97^\circ$), which indicates it not being a hydrogen bond.⁴⁸

In **2b**, the charge of N³ (−0.415 *e*) becomes more negative than in **1b**, due to the interaction with the hydrogen atom (+0.594 *e*). Also, in **2a** the charge of H² is more positive than in **1a** due to the contact with the oxygen of the OH group. Thus, it would be more appropriate to characterize the contact between OH and N³ in **2b** as an attractive electrostatic interaction instead of a hydrogen bond.

In the regioisomer **3a**, one of the methyl group of the TMS moiety is oriented forward of the azide group ($d_{H\cdots N^3} = 2.90$ Å; $\angle CH\cdots N^3 = 121^\circ$), and a bcp is found between N³ and

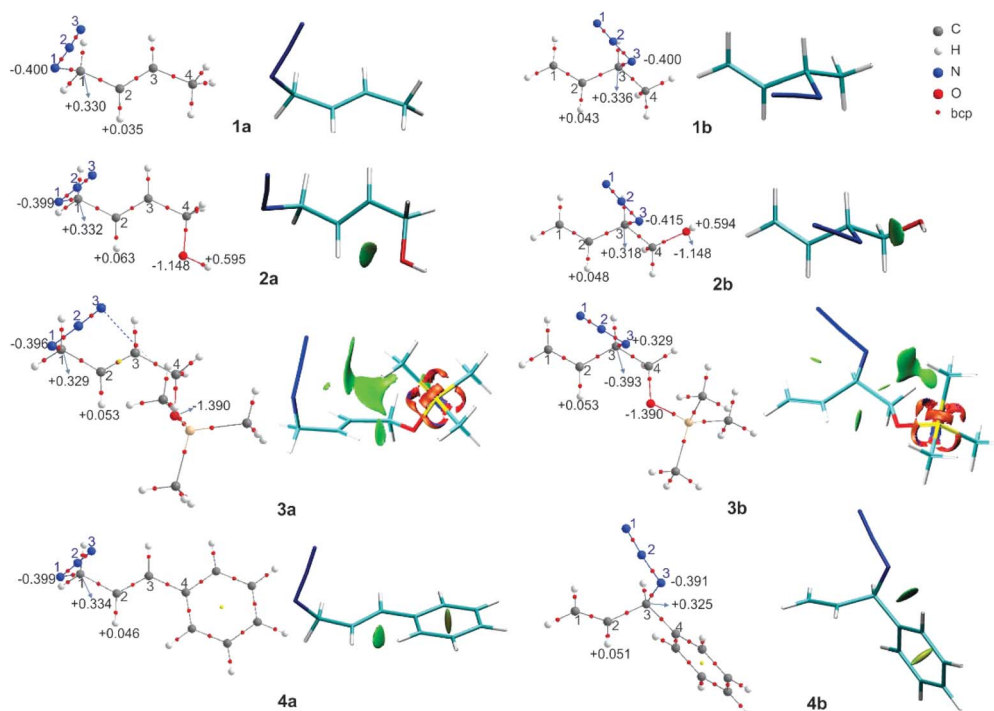


Fig. 2 Molecular graphs of the azides **1–4** (left). For selected atoms, the atomic charges q (e) are given in *e*. NCI gradient isosurfaces (right), represented at an isovalue of 0.5 a.u. and blue-green-red color scale from $-0.05 < \text{sign}(\lambda_2)\rho < +0.05$ a.u.



a hydrogen atom of the TMS. Also, the NCI plot shows a green isosurface between these atoms, denoting a weak interaction. In the regioisomer **3b**, one of the hydrogen atoms of the methyl group of TMS is directed towards N³ ($d_{\text{H}\cdots\text{N}^3} = 3.00 \text{ \AA}$; $\angle\text{CH}\cdots\text{N}^3 = 100^\circ$), but no bcp was found for this interaction, though a green NCI isosurface was visualized. In both **3a** and **3b** regioisomers, there was an attractive interaction between the oxygen atom of the OTMS group and H² ($d_{\text{H}^2\cdots\text{O}} = 2.43 \text{ \AA}$ for **3a**; $d_{\text{H}^2\cdots\text{O}} = 2.54 \text{ \AA}$ for **3b**), reflecting the presence of a green NCI isosurface similar to those found in azide **2**, which might determine the orientation of the C–O bond relative to the double bond. Also, the charges of the H² atom in **3a** and **3b** were more positive than in **1a** and **1b**, respectively, due to the interaction with the oxygen atom of the OTMS group. These weak attractive interactions affect the structure of the regioisomers, whereby in **3a** the bulky TMS group is pointing inside the double bond, while in **3b** it is far off the double bond, making this structure less sterically congested. Therefore, it could be assumed that the structure of **3a** is disfavoured by steric repulsion, which influences the equilibrium distribution.

These interactions that are visualized as a green NCI isosurface between a hydrogen of the phenyl ring and H² ($d_{\text{H}^2\cdots\text{N}} = 2.20 \text{ \AA}$) for **4a** and between a hydrogen of the aromatic ring and N³ in **4b** were repulsive in the first case and attractive in the second. The influence of this kind of interaction was negligible with respect to the conjugative effect, as was established and we will analyse in detail below.

Several stereoelectronic effects contribute to the subtle energy differences. It was stated that populations of regioisomers during the interconversion by the allylic azide rearrangement are governed by stabilization of the C=C bonds with more substitutions.³¹ The nature of the stabilizing interactions, such as donor–acceptor interactions, could be easily rationalized through the NBO analysis.

The hyperconjugative interactions in which $\pi^*\text{C}=\text{C}$ and $\pi\text{C}=\text{C}$ of the double bond of the allylic group act as acceptor and donor orbitals, respectively, were examined according to the second-order perturbation energy ($E^{(2)}$) in the NBO analysis. Also, other selected interactions were analysed. The second order stabilization energies $E^{(2)}$ associated with the most relevant hyperconjugative interactions in the **1–4** azides are summarized in Table 2.

In the primary azides **1–3a** there were hyperconjugative interactions among $\sigma\text{C}^1\text{--N}^1$, $\sigma\text{C}^1\text{--H}^1$, $\sigma\text{C}^4\text{--H}$ donor orbitals and $\pi^*\text{C}^2=\text{C}^3$ antibonding orbital as the acceptor. Also, there was a hyperconjugative interaction $\eta\text{N}^1 \rightarrow \pi^*\text{C}^2=\text{C}^3$ with lower values of $E^{(2)}$. The stronger hyperconjugative effect was associated with the interactions between the two out-of-plane $\sigma\text{C}^4\text{--H}^4$ sigma bonds and the $\pi^*\text{C}^2=\text{C}^3$ antibonding orbital. For **1a** and **2a**, the $E^{(2)}$ of the $\sigma\text{Z}_a \rightarrow \pi^*\text{C}^2=\text{C}^3$ interactions were similar, while it is a little higher for **3a**. For **1a**, when the $\pi\text{C}^2=\text{C}^3$ orbitals acted as donors, the energy of $\pi\text{C}^2=\text{C}^3 \rightarrow \sigma^*\text{Z}_b$ was a little stronger than that for **2a** and **3a**.

The energy of the $\sigma\text{Z}_a \rightarrow \pi^*\text{C}^2=\text{C}^3$ interactions showed a slightly higher value for **1b** and did not justify the shift of the population equilibrium. In **2b**, the $E^{(2)}$ of $\pi\text{C}^2=\text{C}^3 \rightarrow \sigma^*\text{C}^3\text{--N}^3$ and $\pi\text{C}^2=\text{C}^3 \rightarrow \sigma^*\text{C}^3\text{--C}^4$ were slightly more favourable than in

Table 2 Second-order perturbation energies ($E^{(2)}$, kcal mol^{−1}) of the main donor–acceptor interactions in the **1–4** azides^a

Donor	Acceptor	1a	2a	3a	4a
$\sigma\text{C}^1\text{--N}^1$	$\pi^*\text{C}^2=\text{C}^3$	2.91	3.00	3.27	3.13
$\sigma\text{C}^1\text{--H}^1$		4.97	4.98	4.78	4.95
$\sigma\text{C}^4\text{--H}^4$		13.27	13.52	13.40	—
$\sigma\text{C}^4\text{--C}^5$		—	—	—	17.52
ηN^1		1.24	1.29	1.56	1.43
$\sigma\text{Z}_a \rightarrow \pi^*\text{C}^2=\text{C}^3$		22.39	22.79	23.01	27.03
$\pi\text{C}^2=\text{C}^3$	$\sigma^*\text{C}^1\text{--N}^1$	6.65	6.66	6.82	6.58
	$\sigma^*\text{C}^1\text{--H}^1$	2.84	2.71	2.56	2.68
	$\sigma^*\text{C}^4\text{--H}^4$	6.30	6.03	5.96	—
	$\sigma^*\text{C}^4\text{--C}^5$	—	—	—	13.83
$\pi\text{C}^2=\text{C}^3 \rightarrow \sigma^*\text{Z}_b$		15.79	15.40	15.34	23.09
Donor	Acceptor	1b	2b	3b	4b
$\sigma\text{C}^3\text{--N}^3$	$\pi^*\text{C}^1=\text{C}^2$	3.12	3.00	2.92	2.89
$\sigma\text{C}^3\text{--C}^4$		3.42	3.45	3.22	3.17
ηN^1		1.65	1.50	1.32	1.64
$\sigma\text{C}^4\text{--C}^5$		—	—	—	0.59
$\sigma\text{Z}_a \rightarrow \pi^*\text{C}^2=\text{C}^3$		8.19	7.95	7.46	8.29
$\pi\text{C}^1=\text{C}^2$	$\sigma^*\text{C}^3\text{--N}^3$	6.48	6.52	7.08	6.22
	$\sigma^*\text{C}^3\text{--C}^4$	3.18	3.31	3.09	3.10
$\pi\text{C}^1=\text{C}^2 \rightarrow \sigma^*\text{Z}_b$		9.66	9.83	10.17	9.32
ηN^3	$\sigma^*\text{O--H}$	—	0.68	—	—

^a σZ_a and $\sigma^*\text{Z}_b$ denote the bonding and antibonding orbitals that interact with the $\pi^*\text{C}=\text{C}$ and $\pi\text{C}=\text{C}$ orbitals of the allylic group, respectively.

1b. Also, **2b** showed a $\eta\text{N}^1 \rightarrow \sigma^*\text{O--H}$ (0.68 kcal mol^{−1}) interaction, although this only weakly provided stabilization to this regioisomer, as was reported for other systems.⁴⁹

In the secondary azide **3b**, the energy of $\pi\text{C}^1=\text{C}^2 \rightarrow \sigma^*\text{C}^3\text{--N}^3$ was higher than in **1b** by 0.6 kcal mol^{−1}, but the energies of $\pi\text{C}^1=\text{C}^2 \rightarrow \sigma^*\text{C}^3\text{--C}^4$ were quite similar for both. Therefore, the shift in azide **3**'s equilibrium towards the secondary azide, compared with azide **1**, might be explained by the more favourable hyperconjugative $\pi\text{C}^1=\text{C}^2 \rightarrow \sigma^*\text{C}^3\text{--N}^3$ interaction. It was also noticeable that in **3b** there was less steric repulsion than in **3a** due to the orientation of the bulky substituent group.

We might assume that the interactions between the N³ atom and oxygen of the OH and the OTMS groups in **2b** and **3b**, respectively, govern the structure of the molecule, giving a more favourable orbital alignment for the $\pi\text{C}^1=\text{C}^2 \rightarrow \sigma^*\text{C}^3\text{--N}^3$ interaction, *i.e.* both types of interactions act cooperatively to provide more stabilization to these regioisomers.

In the regioisomer **4a**, there were stronger conjugative interactions $\pi\text{C}^4\text{--C}^5 \rightarrow \pi^*\text{C}^2\text{--C}^3$ (17.52 kcal mol^{−1}) and $\pi\text{C}^2\text{--C}^3 \rightarrow \pi^*\text{C}^4\text{--C}^5$ (13.83 kcal mol^{−1}), while in **4b**, these π -conjugation between their vicinal multiple bonds were absent. Thus, the conjugative effect was responsible for the displacement towards the regioisomer **4a**, which was confirmed by the NBO analysis.

Primary vs. tertiary azides

The computed relative energies (ΔG) and the equilibrium ratio for the regioisomers **5–7** are listed in Table 3. In azides **5**, **6** and



Table 3 Relative free energies (ΔG , kcal mol⁻¹) and calculated and experimental equilibrium ratios for the azides under study^a

Azide (X)	R ₁	R ₂	ΔG (X _b – X _a)	X _a : X _b ratio	
				Calcd ^a	Exp. ^b
5	Me	Me	1.45	92 : 8	87 : 2330
6	CH ₂ OH	Me	–0.06	48 : 52	55 : 4522
7	Ph	Me	3.65	100 : 0	100 : 030

^a Ratios were computed using Boltzmann factors based on ΔG . ^b 6a (47% *E-trans*, 8% *Z-cis*).

7, there was an additional methyl group compared with the azides 1, 2 and 4, respectively, and these showed a slight shift towards the primary azides.

The primary azides 5a and 7a were 1.45 and 3.65 kcal mol⁻¹ more stable than the corresponding tertiary isomers, respectively, being the estimated equilibrium ratios concordant with the experimental results. For azide 6, substituted with a hydroxyl group, the difference in energy between the primary and tertiary regioisomer was very small and the calculated ratio slightly favoured the latter in contrast with the experimental result. However, this result reflects an equilibrium shift in azide 6 with respect to azide 5, which is in agreement with the calculated values previously reported.²³

The molecular graphs of azides 5–7 are depicted in Fig. 3 (the topological properties evaluated at the bcps are listed in Table S4 in the ESI†) along with their NCI plots.

All the regioisomers showed a close contact between H¹ and H⁵ ($d_{H^1 \cdots H^5}$, 5a = 2.07 Å, 5b = 2.33 Å, 6a = 2.07 Å, 6b = 2.27 Å, 7a = 2.08 Å, 7b = 2.32 Å), and the NCI plots displayed a green isosurface between them, indicating that it was a weak repulsive interaction. These isosurfaces were larger in the primary azides, in agreement with the distances H¹–H⁵.

In regioisomers 6a and 6b, there was a weak interaction between the oxygen atom of the OH group and H² ($d = 2.39$ and 2.53 Å, respectively), as evidenced by the green isosurface in the NCI plot. Also, the charges of H² in 6a and 6b were more positive than in 5a and 5b, as a consequence of the interaction with the oxygen atom.

In azide 6b, the OH group is directed towards N³ ($d_{H \cdots N} = 2.38$ Å; $\angle OH \cdots N^1 = 107^\circ$), and no bcp was observed between the hydrogen atom of the OH group and the N³, but a green isosurface was found in the NCI plot, indicating a weak interaction. Also, the charges of N³ (–0.403 *e*) and of the hydrogen atom of the OH group (+0.595 *e*) were more negative and positive than those in 5b and 6a, respectively.

In azide 7a, there were repulsive interactions between two hydrogen atoms of the aromatic ring and the H² and a hydrogen of the methyl group (C⁵H₃). While in azide 7b, an attractive interaction between N³ and a hydrogen of the phenyl group was observed. For this interaction, a bcp was found and the topological parameters reflected a weak interaction, in agreement with the green NCI isosurface between both atoms. Thus, the primary azide 7a was disfavoured due to the steric congestion; however, it predominated in the equilibrium as a consequence of the conjugation effect (see below).

The second-order perturbation energy ($E^{(2)}$) values of the relevant hyperconjugative interactions are summarized in Table 4.

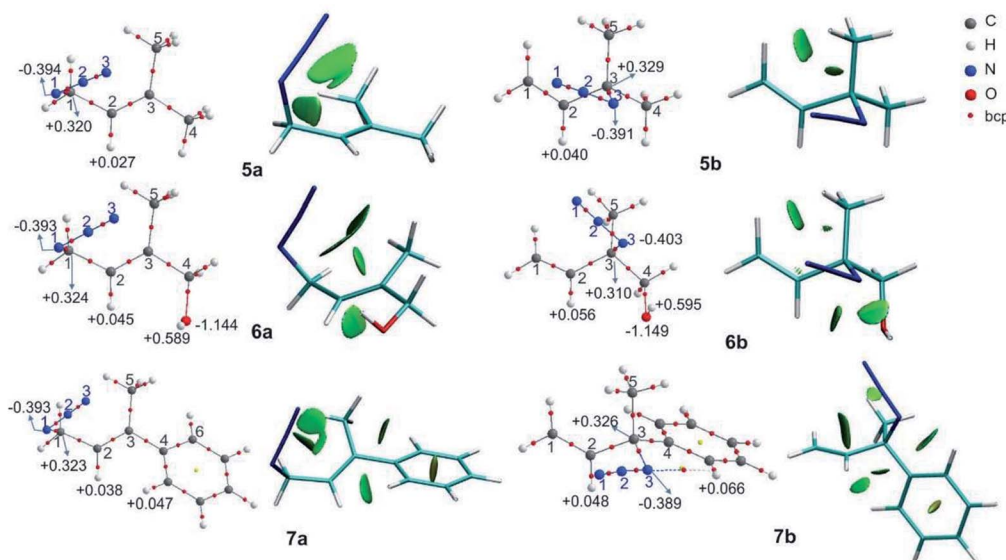


Fig. 3 Molecular graphs of the azides 5–7 (left). For selected atoms, the atomic charges q (e) are given in *e*. NCI gradient isosurfaces (right), represented at an isovalue of 0.5 a.u. and blue-green-red colour scale from $-0.05 < \text{sign}(\lambda_2)\rho < +0.05$ a.u.



Table 4 Second-order perturbation energies ($E^{(2)}$, kcal mol⁻¹) of the main donor–acceptor interactions in the 5–7 azides^a

Donor	Acceptor	5a	6a	7a
σC^1-N^1	$\pi^* C^2=C^3$	2.36	2.42	2.67
σC^1-H^1		5.11	5.14	4.64
σC^4-H^4		14.07	14.12	—
σC^4-C^6				13.17
σC^5-C^7				0.61
σC^5-H^5		15.26	15.27	14.30
ηN^1		0.97	1.03	1.15
$\sigma Z_a \rightarrow \pi^* C^2=C^3$		37.77	37.98	36.54
$\pi C^2=C^3$	$\sigma^* C^1-N^1$	7.48	7.25	7.22
	$\sigma^* C^1-H^1$	2.10	2.06	1.96
	$\sigma^* C^4-H^4$	6.61	5.93	—
	$\sigma^* C^4-C^6$			12.12
	$\sigma^* C^5-C^7$			1.02
	$\sigma^* C^5-H^5$	5.91	5.90	5.67
$\pi C^2=C^3 \rightarrow \sigma Z_b$		22.10	21.14	27.99
Donor	Acceptor	5b	6b	7b
σC^3-N^3	$\pi^* C^1=C^2$	3.23	3.19	3.31
σC^3-C^4		3.76	3.60	3.25
ηN^1		1.69	1.61	1.73
$\sigma Z_a \rightarrow \pi^* C^2=C^3$		8.68	8.40	8.28
$\pi C^1=C^2$	$\sigma^* C^3-N^3$	6.01	7.01	5.82
	$\sigma^* C^3-C^4$	3.28	2.96	3.40
$\pi C^1=C^2 \rightarrow \sigma Z_b$		9.29	9.97	9.22
ηN^3	$\sigma^* O-H$		0.65	—

^a σZ_a and $\sigma^* Z_b$ denote the bonding and antibonding orbitals that interact with the $\pi^* C=C$ and $\pi C=C$ orbitals of the allylic group, respectively.

In the primary azides **5a** and **6a**, there were stronger hyper-conjugative interactions between the two out-of-plane σC^4-H^4 and σC^5-H^5 orbitals and the $\pi^* C^2=C^3$ antibonding orbital, and the energies of interaction $\sigma Z_a \rightarrow \pi^* C^2=C^3$ for **5a** (37.77 kcal mol⁻¹) and **6a** (37.98 kcal mol⁻¹) were substantially similar.

The interactions wherein the $\pi C^2=C^3$ acts as the donor orbital were a little stronger in **5a** than in **6a**, particularly the $\pi C^2=C^3 \rightarrow \sigma C^4-H^4$ interactions. In **5a**, the $\sigma^* C^4-H^4$ orbitals were better aligned to interact with the $\pi C^2=C^3$ donor orbital, while in **6a** the contact between the oxygen atom of the OH group and H^2 affected the orientation of these orbitals, and thus the overlap among them. Thus, the values of $E^{(2)}$ for the $\pi C^2=C^3 \rightarrow \sigma Z_b$ interactions were slightly higher in azide **5a**.

Comparing the energies of $\sigma Z_a \rightarrow \pi^* C^2=C^3$ and $\pi C^2=C^3 \rightarrow Z_b$ between azides **5a**, **6a** and **1a**, **2a**, those of **5a**, **6a** considerably higher, which clearly demonstrated the relevance of the hyper-conjugation, as reflected in the equilibrium ratio.

In the tertiary azides **5b** and **6b** the energies of $\sigma Z_a \rightarrow \pi^* C^2=C^3$ were almost similar. When the $\pi C^1=C^2$ orbital acted as a donor, the energies of $\pi C^1=C^2 \rightarrow \sigma^* Z_b$ were higher in **6b**, particularly the $\pi C^1=C^2 \rightarrow \sigma^* C^3-N^3$ interaction, which was stronger by 1 kcal mol⁻¹ than in **5b**. Also, in **6b**, the interaction $\eta N^3 \rightarrow \sigma^* O-H$ (0.65 kcal mol⁻¹) was found, as in azide **2b**. The stabilizing $\eta N^3 \rightarrow \sigma^* O-H$ interaction led to a better $\pi C^1=C^2 \rightarrow$

$\sigma^* C^3-N^3$ orbital orientation for their overlap, and thus both interactions contributed to stabilizing the regioisomer **6b**.

In **7a**, the phenyl group is twisted out of the plane to relieve the repulsive interaction with the methyl (C^5H_3) group ($C^2-C^3-C^4-C^6 = 37^\circ$) and this disrupted the conjugation. A stronger $\pi C^4=C^6 \rightarrow \pi^* C^2=C^3$ interaction (13.17 kcal mol⁻¹) and another weak $\pi C^5-C^7 \rightarrow \pi^* C^2=C^3$ (0.61 kcal mol⁻¹) were found, but the energy of $\sigma Z_a \rightarrow \pi^* C^2=C^3$ was lower than those for azides **5a** and **6a**. When $\pi C^2=C^3$ acted as an orbital donor, a stronger conjugation was found for $\pi C^2=C^3 \rightarrow \pi^* C^4=C^6$ (12.12 kcal mol⁻¹), with the energies of $\pi C^2=C^3 \rightarrow \sigma^* Z_b$ (27.99 kcal mol⁻¹) being higher than in **5a** and **6a**. Also, in **7b**, the energies of $\sigma Z_a \rightarrow \pi^* C^2=C^3$ and $\pi C^1=C^2 \rightarrow Z_b$ were weaker than in **5b** and **6b**.

Although the conjugation energy of **7a** was weakened by geometric constraints and it was decreased compared to that in **4b**, it was still strong enough to explain the observed equilibrium shift.

Secondary vs. tertiary azides

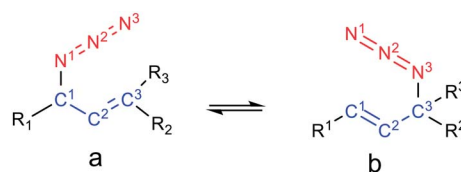
The relative free energies (ΔG) and the equilibrium ratios for the regioisomers **8–12** are listed in Table 5. The molecular graphs of the azides **8–10** are depicted in Fig. 4 along with their NCI plots. (For the remaining azides, see the ESI†).

The secondary azides **8a** and **9a** were more stable than their corresponding tertiary regioisomers by 0.6 and 1.9 kcal mol⁻¹, respectively; therefore, the more substituted alkene isomers were thermodynamically favoured, as stated previously.³¹ This is the reverse for azides **10**, **11** and **12**, being secondary regioisomers less stable by 0.3, 1.0 and 3.6 kcal mol⁻¹ than their tertiary counterparts, respectively. Overall, the calculated equilibrium ratios acceptably reproduced the experimental results

Table 5 Relative free energies (ΔG , kcal mol⁻¹) and calculated and experimental equilibrium ratios for the azides under study^a

Azide (X)	R ₁	R ₂	R ₃	ΔG ($X_b - X_a$)	$X_a : X_b$ ratio	
					Calcd ^a	Exp. ^{b,c}
8	Me	Me	Me	0.57	72 : 28	65 : 35 (ref. 22)
9	CH ₂ OH	Me	Me	1.93	96 : 4	82 : 18 (ref. 22)
10	Me	CH ₂ OH	Me	-0.31	37 : 63	36 : 64 (ref. 50)
11	cHex	CH ₂ OH	Me	-1.03	15 : 85	37 : 63 (ref. 50)
12	Ph	CH ₂ OH	Me	-3.6	0 : 100	0 : 100 (ref. 50)

^a Ratios were computed using Boltzmann factors based on ΔG . ^b **8b** (32% *trans*, 3% *cis*). ^c The experimental data given correspond to a structurally similar allylic azide to **12**, wherein the aromatic group is 2-pyridyl instead phenyl.



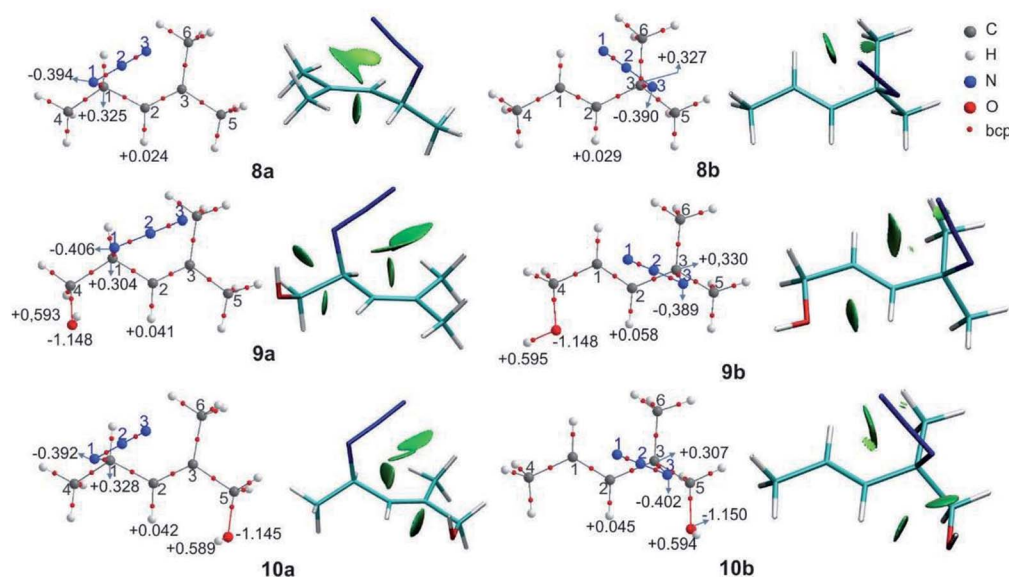


Fig. 4 Molecular graphs of the azides **8–10** (left). For selected atoms, the atomic charges q (Ω) are given in e. NCI gradient isosurfaces (right), represented at an isovalue of 0.5 a.u. and blue-green-red colour scale from $-0.05 < \text{sign}(\lambda_2)\rho < +0.05$ a.u.

and reflected the observed regioisomer population composition changes with respect to azide **8**.

In azide **9a**, the OH group is directed towards N^1 ($d_{H\cdots N} = 2.38$ Å; $\angle OH\cdots N^1 = 106^\circ$), and in azides **10–12b** it points towards N^3 ($d_{H\cdots N} = 2.33$ Å; $\angle OH\cdots N^3 = 106^\circ$), forming a stabilizing weak interaction, as denoted by a green NCI isosurface. Again, from the molecular graphs, no bcp was observed between the hydrogen atom of the OH group and N^1 in azide **9a** and N^3 in azides **10–12b**.

In **9a** and **9b**, the negative/positive charges of the O/H atoms of the OH group were similar; nevertheless, the negative charge of N^1 in **9a** was higher than that in the other secondary azides. In **10b**, the positive/negative charges of the H/O atoms of the OH group were augmented with respect to those in **10a**. Also, the negative charge of N^3 in **10b** was higher than that in **8b** and **9b**. Similar results were found for azides **11b** and **12b**. Thus, the polarization of the O–H bond and the increase in the electronic population in N^3 arise from the contact between these atoms. In all the regioisomers, a contact between the oxygen atom and H^2 was visualized by a green NCI isosurface.

The second-order perturbation energy of the relevant hyperconjugative interactions are summarized in Table 6.

From the NBO analysis, it was observed that in the secondary azides **8–12a**, there were hyperconjugative interactions among the donor σC^1-N^1 , σC^1-C^4 , σC^5-H^5 and σC^6-H^6 and the $\pi C^2=C^3$ antibonding orbital as the acceptor. In **9a**, a weak $\sigma C^1-H^1 \rightarrow \pi C^2=C^3$ interaction (0.74 kcal mol $^{-1}$) and in **11a** a $\sigma C^4-C \rightarrow \pi C^2=C^3$ interaction (0.61 kcal mol $^{-1}$) were also found due to their orientation. The energies of the $\sigma Z_a \rightarrow \pi C^2=C^3$ interactions were similar for the secondary azides and do not explain the observed changes in the equilibrium populations.

There are some significant differences in energies when the orbital $\pi C^2=C^3$ acts as a donor. Overall, the $\pi C^2=C^3 \rightarrow \sigma^* Z_b$

interactions were weaker in azides **10–12a** than in **8a** (by about 1.5 kcal mol $^{-1}$), particularly the $\pi C^2=C^3 \rightarrow \sigma^* C^5-H^5$ interactions. In azides **10–12a** the OH group is attached to C^5 and this

Table 6 Second-order perturbation energies ($E^{(2)}$, kcal mol $^{-1}$) of the main donor–acceptor interactions in the **8–12** azides

Donor	Acceptor	8a	9a	10a	11a	12a
σC^1-N^1	$\pi^* C^2=C^3$	2.36	2.17	2.47	2.56	2.31
σC^1-C^4		3.25	3.14	3.26	2.74	2.88
σC^1-H^1			0.74			
σC^5-H^5		14.08	14.20	14.12	14.22	14.12
σC^6-H^6		15.34	15.32	15.30	15.33	15.30
ηN^1		1.15	0.81	1.22	1.32	1.26
σC^3-C^4					0.61	
$\sigma Z_a \rightarrow \pi^* C^2=C^3$		36.18	36.38	36.37	36.78	35.87
$\pi C^2=C^3$	$\sigma^* C^1-N^1$	7.74	8.42	7.45	7.56	7.21
	$\sigma^* C^1-C^4$	2.20	1.81	2.31	2.27	2.47
	$\sigma^* C^1-H^1$	0.58	0.98			
	$\sigma^* C^5-H^5$	6.65	6.58	5.96	5.99	5.88
	$\sigma^* C^6-H^6$	5.92	5.93	5.82	5.79	5.78
$\pi C^2=C^3 \rightarrow \sigma^* Z_b$		23.09	23.72	21.54	21.61	21.34
Donor	Acceptor	8b	9b	10b	11b	12b
σC^3-N^3	$\pi^* C^1=C^2$	3.07	3.16	3.02	3.16	3.06
σC^3-C^6		3.66	3.67	3.50	3.55	3.87
σC^4-H^4		13.26	13.61	13.32		
ηN^1		1.53	1.56	1.43	1.42	1.44
σC^4-C					8.83	17.65
$\sigma Z_a \rightarrow \pi^* C^2=C^3$		21.52	22.00	21.27	16.96	26.02
$\pi C^1=C^2$	$\sigma^* C^3-N^3$	6.56	6.49	7.69	8.01	7.09
	$\sigma^* C^3-C^5$	3.40	3.32	3.03	2.90	3.17
	$\sigma^* C^4-H^4$	6.37	6.09	6.32		
	$\sigma^* C^4-C$				6.43	14.16
$\pi C^1=C^2 \rightarrow \sigma^* Z_b$		16.33	15.90	17.04	17.34	24.42
ηN^3	$\sigma^* O-H$			0.69	0.66	0.66



might affect the $\pi\text{C}^2=\text{C}^3 \rightarrow \sigma^*\text{C}^5-\text{H}^5$ interaction. The $\pi\text{C}^2=\text{C}^3 \rightarrow \sigma^*\text{C}^1-\text{H}^1$ interaction was only found in azides **10a** and **11a**. For azide **9a**, $\pi\text{C}^2=\text{C}^3 \rightarrow \sigma^*\text{N}^1-\text{C}^1$ was slightly stronger, which might be a consequence of the contact between the hydrogen atom of the OH group and the N^1 atom, even though for this case no hyperconjugation interaction was found. Thus, the strength of the hyperconjugative interactions in which the $\pi\text{C}^2=\text{C}^3$ act as donor orbital decrease when the CH_2OH group is attached to one carbon atom of the double bond.

In the tertiary azides **8b–12b**, there were hyperconjugative interactions among the $\sigma\text{C}^3-\text{N}^3$, $\sigma\text{C}^3-\text{C}^5$ orbital donor and $\pi^*\text{C}^1=\text{C}^2$ orbital acceptor. Also, azides **8b–10b** displayed $\sigma\text{C}^4-\text{H}^4 \rightarrow \pi^*\text{C}^1=\text{C}^2$ interactions, while **11b** and **12b** showed $\sigma\text{C}^4-\text{C} \rightarrow \pi^*\text{C}^1=\text{C}^2$ interactions involving the cyclic substituent. The $\sigma\text{C}^4-\text{C} \rightarrow \pi^*\text{C}^1=\text{C}^2$ interaction in azide **11b** had a lower energy than similar interactions in the other azides, but this did not explain the predominance of the regioisomer **11b** in the equilibrium mixture. Also, the energies of $\sigma\text{Z}_a \rightarrow \pi^*\text{C}^2=\text{C}^3$ did not reflect the trend of the tertiary azides population in the equilibrium mixture.

The hyperconjugative energies in **9b**, wherein the $\pi\text{C}^1=\text{C}^2$ acts as a donor orbital, were slightly weaker than in **8b**, due to the CH_2OH being attached to the double bond, as was mentioned above.

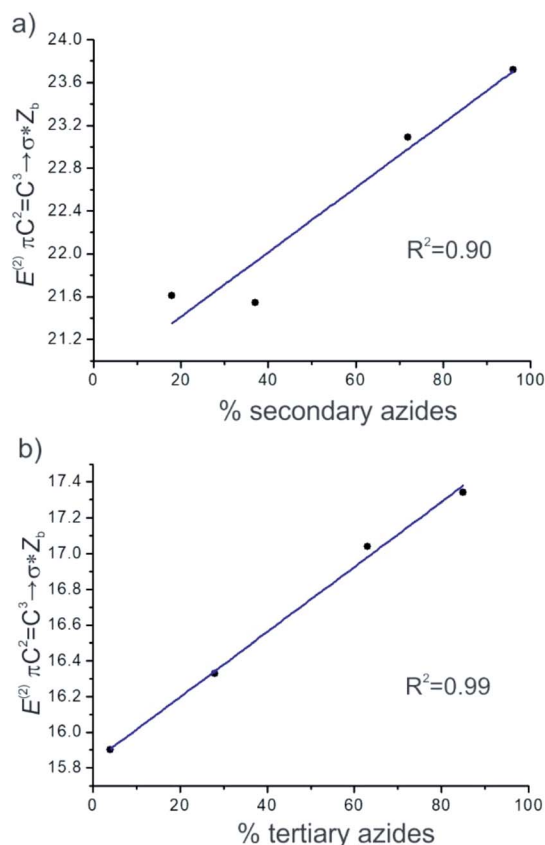


Fig. 5 Plots of the correlation between (a) the hyperconjugation energies $E^{(2)} \pi\text{C}^2=\text{C}^3 \rightarrow \sigma^*\text{Z}_b$ and the percentage of secondary azides and (b) $E^{(2)} \pi\text{C}^1=\text{C}^2 \rightarrow \sigma^*\text{Z}_b$ and the percentage of tertiary azides in the equilibrium mixture.

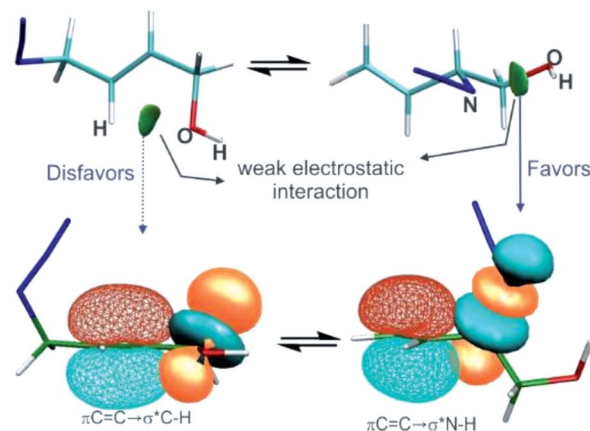


Fig. 6 The interplay of the electrostatic interactions (top, visualised through NCI gradient isosurfaces at an isovalue = 0.5) and hyperconjugative interactions (bottom, displayed by natural bond orbitals at an isovalue = 0.05) in azide regioisomers substituted with a hydroxyl group.

The energies of $\pi\text{C}^1=\text{C}^2 \rightarrow \sigma^*\text{Z}_b$ were higher in **10b** and **11b** than in **8a**, mainly because of the strengthening of the $\pi\text{C}^1=\text{C}^2 \rightarrow \sigma^*\text{C}^3-\text{N}^3$ interaction (by 1.13 and 1.45 kcal mol⁻¹, respectively). In both **10b** and **11b**, $\eta\text{N}^3 \rightarrow \sigma^*\text{O}-\text{H}$ interactions (0.69 and 0.66 kcal mol⁻¹, respectively) were also found. This interaction, besides being a stabilizing one, also affects the orientation of the regioisomers, favouring the overlap of the $\pi\text{C}^1=\text{C}^2$ and $\sigma\text{C}^3-\text{N}^3$ orbitals.

It was noted that the greater the energies of $\pi\text{C}^2=\text{C}^3 \rightarrow \sigma^*\text{Z}_b$ and $\pi\text{C}^1=\text{C}^2 \rightarrow \sigma^*\text{Z}_b$, the more the equilibrium was shifted to the secondary and tertiary azides isomers, respectively. A good linear correlation between $E^{(2)} \pi\text{C}^2=\text{C}^3 \rightarrow \sigma^*\text{Z}_b$ and the calculated percentage of secondary azides was obtained for azides **8–11** ($R^2 = 0.90$). Also, a better linear correlation between $E^{(2)} \pi\text{C}^1=\text{C}^2 \rightarrow \sigma^*\text{Z}_b$ and the percentage of tertiary azides was found ($R^2 = 0.99$) (Fig. 5).

According to these results, the hyperconjugative interactions in which the double bond acts as a donor were the main factors that controlled the stabilization of the regioisomers, and therefore the distribution of the regioisomers in the equilibrium mixture, although other electrostatic interactions may also influence the process.

In azide **12a**, the energies of the $\pi\text{C}^1=\text{C}^2 \rightarrow \sigma^*\text{C}^3-\text{N}^3$ and $\pi\text{C}^2=\text{C}^3 \rightarrow \sigma^*\text{Z}_b$ interactions were the lowest. The conjugated azide **12b** was greatly stabilized by the conjugative interactions $\text{C}^4-\text{C} \rightarrow \pi^*\text{C}^1=\text{C}^2$ (17.65 kcal mol⁻¹) and $\pi\text{C}^1=\text{C}^2 \rightarrow \sigma\text{C}^4-\text{C}$ (14.16 kcal mol⁻¹). Also, there was an interaction $\eta\text{N}^3 \rightarrow \sigma^*\text{O}-\text{H}$, which favoured the $\pi\text{C}^1=\text{C}^2 \rightarrow \sigma\text{C}^3-\text{N}^3$ interaction. Both interactions contributed to stabilizing the structure, but the governing factor in this case was the conjugative effect.

Conclusions

In this work, several representative allylic azides with different degrees of substitution on the double bond were studied using density functional theory and QTAIM, NCI, and NBO



approaches in order to evaluate the factors responsible for their stabilities and therefore to explain the observed equilibrium shift.

The results revealed that when the azides were substituted with OH groups or heteroatoms, weak electrostatic interactions could be evidenced in each regioisomer that influence the conformation and thus the hyperconjugative interactions (Fig. 6).

In the regioisomer in which the substituent group was attached to a carbon atom of the double bond, an interaction was formed between the O atom of the OH group and an H atom of the allylic moiety and this weakened the hyperconjugation $\pi\text{C}=\text{C} \rightarrow \sigma^*\text{Z}_b$. In the other regioisomer, the OH group was close to the azide group, and an interaction was observed between them which gave a more favourable orbital alignment for the negative hyperconjugative interaction $\pi\text{C}=\text{C} \rightarrow \sigma^*\text{Z}_b$. The analysis of the charge density distribution showed that the interaction between the OH group and a nitrogen atom of the azide group showed the characteristic of an electrostatic attractive interaction, rather than a hydrogen bond as was previously proposed and this was attributed to be responsible for the observed equilibrium shift.

The equilibrium shift could not be explained by a specific interaction in one of the regioisomers, instead it was due to a combination of two opposite effects: weakening and strengthening of the hyperconjugation promoted by the electrostatic interactions involving the substituent group.

Therefore, hyperconjugative interactions were found to play a primary role in the regioisomers stability. A good linear correlation was obtained for the secondary and tertiary azides in equilibrium between the hyperconjugative energies of $\pi\text{C}=\text{C} \rightarrow \sigma^*\text{Z}_b$ and the calculated percentage of secondary and tertiary azides. Also, it was observed that other effects, such as steric effects, influenced the stability of the regioisomers.

For the azides substituted with an aromatic ring, the energy of the conjugative interactions provided a great stabilization to the conjugated regioisomer and this was enough to explain its exclusive existence in the equilibrium mixture. This effect dominated over other kinds of interactions, such as electrostatic interactions or steric factors.

This study not only provides insights into the factor controlling the stabilities of substituted allylic azides, but also allows one to predict which regioisomer will be predominant in the equilibrium mixture.

Conflicts of interest

There are no conflicts to declare.

Acknowledgements

The authors are members of the Research Career of CONICET-Argentina. This work was supported in part by grants from the UNNE (Universidad Nacional del Nordeste), SECY-UNNE (PI: No. 17F014), Agencia Nacional de Promoción Científica y Tecnológica, ANPCyT-Argentina (PICT 2014-3693 and PICT-2015-2635) and Universidad Nacional de Rosario (BIO 503).

Notes and references

- 1 E. F. V. Scriven and K. Turnbull, *Chem. Rev.*, 1988, **88**, 297–368.
- 2 S. Bräse, C. Gil, K. Knepper and V. Zimmermann, *Angew. Chem., Int. Ed.*, 2005, **44**, 5188–5240.
- 3 P.-G. Ding, X.-S. Hu, F. Zhou and J. Zhou, *Org. Chem. Front.*, 2018, **5**, 1542–1559.
- 4 V. V. Rostovtsev, L. G. Green, V. V. Fokin and K. B. Sharpless, *Angew. Chem., Int. Ed.*, 2002, **41**, 2596–2599.
- 5 C. W. Tornøe, C. Christensen and M. Meldal, *J. Org. Chem.*, 2002, **67**, 3057–3064.
- 6 E.-C. Liu and J. J. Topczewski, *J. Am. Chem. Soc.*, 2019, **141**, 5135–5138.
- 7 S. Schricker, M. Palacio, B. T. Thirumamagal and B. Bhushan, *Ultramicroscopy*, 2010, **110**, 639–649.
- 8 E. M. Sletten and C. R. Bertozzi, *Angew. Chem., Int. Ed.*, 2009, **48**, 6974–6998.
- 9 T. Zheng, S. H. Rouhanifard, A. S. Jalloh and P. Wu, *Top. Heterocycl. Chem.*, 2012, **28**, 163–183.
- 10 D. Dheer, V. Singh and R. Shankar, *Bioorg. Chem.*, 2017, **71**, 30–54.
- 11 R. H. Vekariya, R. Liu and J. Aubé, *Org. Lett.*, 2014, **16**, 1844–1847.
- 12 R. Liu, O. Gutierrez, D. J. Tantillo and J. Aubé, *J. Am. Chem. Soc.*, 2012, **134**, 6528–6531.
- 13 A. S. Carlson and J. J. Topczewski, *Org. Biomol. Chem.*, 2019, **17**, 4406–4429.
- 14 A. A. Ott and J. J. Topczewski, *Arkivoc*, 2019, 1–17.
- 15 A. Gagneux, S. Winstein and W. G. Young, *J. Am. Chem. Soc.*, 1960, **82**, 5956–5957.
- 16 A. Gagneux, S. Winstein and W. G. Young, *J. Org. Chem.*, 1969, **1**, 5956–5957.
- 17 C. A. VanderWerf and V. L. Heasley, *J. Org. Chem.*, 1966, **31**, 3534–3537.
- 18 W. J. L. Noble, *J. Phys. Chem.*, 1963, **67**, 2451–2453.
- 19 A. Padwa and M. M. Sá, *Tetrahedron Lett.*, 1997, **38**, 5087–5090.
- 20 A. A. Ott, M. H. Packard, M. A. Ortuno, A. Johnson, V. P. Suding, C. J. Cramer and J. J. Topczewski, *J. Org. Chem.*, 2018, **83**, 8214–8224.
- 21 B. M. Trost and S. R. Pulley, *Tetrahedron Lett.*, 1995, **36**, 8737–8740.
- 22 A. K. Feldman, B. Colasson, K. B. Sharpless and V. V. Fokin, *J. Am. Chem. Soc.*, 2005, **127**, 13444–13445.
- 23 A. Jabbari, *Org. Chem. J.*, 2010, **1**, 6–14.
- 24 S. Adachi, A. B. Cognetta, M. J. Niphakis, Z. He, A. Zajdlík, J. D. S. Denis, C. C. G. Scully, B. F. Cravatt and A. K. Yudin, *Chem. Commun.*, 2015, **51**, 3608–3611.
- 25 M. H. Packard, J. H. Cox, V. P. Suding and J. J. Topczewski, *Eur. J. Org. Chem.*, 2017, 6365–6368.
- 26 J. S. Panek, M. Yang and I. Muler, *J. Org. Chem.*, 1992, **57**, 4063–4064.
- 27 A. Hassner, R. Fibiger and D. Andisik, *J. Org. Chem.*, 1984, **49**, 4237–4244.



- 28 R. F. W. Bader, *Atoms in Molecules. A Quantum Theory*, Oxford Science Publications, Clarendon Press, London, 1990.
- 29 C. F. Matta and R. J. Boyd, *The quantum theory of atoms in molecules: from solid state to DNA and drug design*, Wiley-VCH, Weinheim, 2007.
- 30 E. O. J. Porta, M. M. Vallejos, A. B. J. Bracca and G. R. Labadie, *RSC Adv.*, 2017, **7**, 47527–47538.
- 31 K. Han-Young and K. Y. Kee, *Bull. Korean Chem. Soc.*, 2017, **38**, 1419–1426.
- 32 F. Weinhold and C. R. Landis, *Valency and bonding: a natural bond orbital donor-acceptor perspective*, Cambridge University Press, UK, 2005.
- 33 P. L. A. Popelier, *Atoms in Molecules. An Introduction*, Pearson Education, Harlow, UK, 2000.
- 34 Y. Zhao and D. Truhlar, *Theor. Chem. Acc.*, 2008, **120**, 215–241.
- 35 A. V. Marenich, C. J. Cramer and D. G. Truhlar, *J. Phys. Chem. B*, 2009, **113**, 6378–6396.
- 36 A. D. Becke, *J. Chem. Phys.*, 1993, **98**, 5648–5652.
- 37 C. Lee, W. Yang and R. G. Parr, *Phys. Rev. B: Condens. Matter Mater. Phys.*, 1988, **37**, 785–789.
- 38 B. J. Lynch, P. L. Fast, M. Harris and D. G. Truhlar, *J. Phys. Chem. A*, 2000, **104**, 4811–4815.
- 39 T. A. Keith, *AIMAll, Version 11.12*, TK Gristmill Software, Overland Park KS, USA, 19th edn, 2011.
- 40 J. Contreras-García, E. R. Johnson, S. Keinan, R. Chaudret, J.-P. Piquemal, D. N. Beratan and W. Yang, *J. Chem. Theory Comput.*, 2011, **7**, 625–632.
- 41 M. J. Frisch, G. W. Trucks, H. B. Schlegel, G. E. Scuseria, M. A. Robb, J. R. Cheeseman, G. Scalmani, V. Barone, G. A. Petersson, H. Nakatsuji, X. Li, M. Caricato, A. Marenich, J. Bloino, B. G. Janesko, R. Gomperts, B. Mennucci, H. P. Hratchian, J. V. Ortiz, A. F. Izmaylov, J. L. Sonnenberg, D. Williams-Young, F. Ding, F. Lipparini, F. Egidi, J. Goings, B. Peng, A. Petrone, T. Henderson, D. Ranasinghe, V. G. Zakrzewski, J. Gao, N. Rega, G. Zheng, W. Liang, M. Hada, M. Ehara, K. Toyota, R. Fukuda, J. Hasegawa, M. Ishida, T. Nakajima, Y. Honda, O. Kitao, H. Nakai, T. Vreven, K. Throssell, J. A. Montgomery Jr, J. E. Peralta, F. Ogliaro, M. Bearpark, J. J. Heyd, E. Brothers, K. N. Kudin, V. N. Staroverov, T. Keith, R. Kobayashi, J. Normand, K. Raghavachari, A. Rendell, J. C. Burant, S. S. Iyengar, J. Tomasi, M. Cossi, J. M. Millam, M. Klene, C. Adamo, R. Cammi, J. W. Ochterski, R. L. Martin, K. Morokuma, O. Farkas, J. B. Foresman and D. J. Fox, *Gaussian 09, Revision D.01*, Gaussian, Inc., Wallingford CT, 2009.
- 42 Y. Yang, C. Qu, X. Chen, K. Sun, L. Qu, W. Bi, H. Hu, R. Li, C. Jing, D. Wei, S. Wei, Y. Sun, H. Liu and Y. Zhao, *Org. Lett.*, 2017, **19**, 5864–5867.
- 43 E. Arunan, G. R. Desiraju, R. A. Klein, J. Sadlej, S. Scheiner, I. Alkorta, D. C. Clary, R. H. Crabtree, J. J. Dannenberg, P. Hobza, H. G. Kjaergaard, A. C. Legon, B. Mennucci and D. J. Nesbitt, *Pure Appl. Chem.*, 2011, **83**, 1637–1641.
- 44 J. R. Lane, J. Contreras-García, J.-P. Piquemal, B. J. Miller and H. G. Kjaergaard, *J. Chem. Theory Comput.*, 2013, **9**, 3263–3266.
- 45 E. R. Johnson, S. Keinan, P. Mori-Sánchez, J. Contreras-García, A. J. Cohen and W. Yang, *J. Am. Chem. Soc.*, 2010, **132**, 6498–6506.
- 46 D. L. Thomsen, J. L. Axson, S. D. Schröder, J. R. Lane, V. Vaida and H. G. Kjaergaard, *J. Phys. Chem. A*, 2013, **117**, 10260–10273.
- 47 R. E. Rosenberg, *J. Phys. Chem. A*, 2019, **123**, 7651–7660.
- 48 L. Estévez and R. A. Mosquera, *J. Phys. Chem. A*, 2007, **111**, 11100–11109.
- 49 M. M. Vallejos, E. L. Angelina and N. M. Peruchena, *J. Phys. Chem. A*, 2010, **114**, 2855–2863.
- 50 D. Craig, J. W. Harvey, A. G. O'Brien and A. J. P. White, *Org. Biomol. Chem.*, 2011, **9**, 7057–7061.

